Theory of ionization-induced trapping in laser-plasma accelerators

M. Chen, E. Esarey,[a] C. B. Schroeder, C. G. R. Geddes, and W. P. Leemans
Lawrence Berkeley National Laboratory, Berkeley, California 94720, USA

(Received 27 November 2011; accepted 31 January 2012; published online 5 March 2012)

Ionization injection in a laser-plasma accelerator is studied analytically and by multi-dimensional particle-in-cell (PIC) simulations. To enable the production of low energy spread beams, we consider a short region containing a high atomic number gas (e.g., nitrogen) for ionization-induced trapping, followed by a longer region using a low atomic number gas (e.g., hydrogen), that is, free of additional trapping, for post acceleration. For a broad laser pulse, ionization injection requires a minimum normalized laser field of $a_0 \simeq 1.7$, assuming a resonant Gaussian laser pulse. Effects of gas mix parameters, including species, concentration, and length of the mixture region, on the final electron injection number and beam quality are studied. The minimum energy spread is determined by the spread in initial ionized phases of the electrons in the wakefield due to the tunneling ionization process within the laser pulse. Laser polarization and intensity effects on injection number and final electron emittance are examined. Two-dimensional PIC simulations are used to study the ionization injection process and the transverse beam structure. With proper laser-plasma parameters, mono-energetic electron beams with 10 pC charge, a central energy at GeV level, and energy spread less than 1% can be produced in a mixed gas with ionized electron density of $10^{18}\,\mathrm{cm}^{-3}$. Lower density can give a higher final accelerated beam energy and reduce the final relative energy spread even further. © *2012 American Institute of Physics*. [http://dx.doi.org/10.1063/1.3689922]

I. INTRODUCTION

Laser-plasma accelerators[1] are of great interest because of their ability to sustain extremely large acceleration gradients, enabling compact accelerating structures. Laser-plasma acceleration is realized by using a high-intensity laser to ponderomotively drive a large plasma wave (or wakefield) in an underdense plasma. The plasma wave has relativistic phase velocity and can support large electric fields in the direction of propagation of the laser. When the laser pulse is near resonant (laser duration on the order of the plasma period) and the laser intensity is relativistic, with normalized laser vector potential $a = eA/m_e c^2 \sim 1$, the size of the accelerating field is on the order of $E_0 = cm_e\omega_p/e$ or $E_0(\mathrm{V/m}) \simeq 96\sqrt{n_0(\mathrm{cm}^{-3})}$, where $\omega_p = (4\pi n_0 e^2/m_e)^{1/2}$ is the electron plasma frequency, n_0 is the ambient electron number density, m_e and e are the electron rest mass and charge, respectively, and c is the speed of light in vacuum. In addition to extremely large accelerating gradients, plasma-based accelerators have the potential to produce extremely short electron bunches, a fraction of the plasma wavelength $\lambda_p = 2\pi c/\omega_p = 2\pi/k_p$. Therefore, laser-plasma accelerators are actively being investigated as ultra-compact sources of high-brightness beams for the next generation of light sources[2,3] and linear colliders.[4]

High-quality electron beams up to 1 GeV have been experimentally demonstrated in cm-scale plasma channels.[5,6] In these channel-guided experiments, the electron beam was created by trapping (self-injection) of background plasma electrons in the plasma wave. Both the quality and stability of the laser-plasma accelerated electron beams can be improved by using triggered injection methods to control the amount of trapped charge and the initial phase-space characteristics. Both laser-triggered methods[7–10] and plasma density tailoring[11–13] have been proposed for controlled injection. Triggered injection into accelerating plasma waves via colliding laser pulses has been demonstrated experimentally.[14–16] Production of electron beams via plasma wave excitation on a negative density gradient has also been achieved.[17–21]

Injection of background plasma electrons may also be achieved via laser ionization.[22–26] Injection of electrons is achieved by ionizing deeply bound electrons from a high atomic number (Z) gas at a proper phase inside the laser-driven wakefield, allowing them to be trapped in the wakefield. Chen *et al.*,[23] previously analyzed a method for ionization injection by using of two orthogonally directed laser pulses and a gaseous medium with a moderate or high atomic number (e.g., neon). A pump laser pulse ionizes the medium to its mid-charge states to form underdense plasma and, subsequently, excites a large amplitude plasma wave. Another ultrashort laser pulse with higher intensity is then injected transversely, which further ionizes the medium to high-charge states producing unbound electrons. The newly ionized electrons can be trapped in the plasma wave and accelerated to high energies.

Ionization induced trapping has been realized experimentally using a single laser pulse by ionizing electrons in the wakefield near the peak of the laser field.[24–26] However, the final electron energy spread was quite large in these experiments. This is the case since these experiments used a single mixed gas that resulted in continuous injection over the laser-plasma interaction region and, hence, resulted in a large beam energy spread.

[a]Electronic mail: EHEsarey@lbl.gov.

In this paper, we examine the physics of ionization injection produced by a single, intense ($>10^{18}$ W/cm^2) laser pulse propagating through a gas mixture consisting primarily of a low Z gas (e.g., 99% hydrogen) with a small amount of high Z gas (e.g., 1% nitrogen). The leading edge of the laser pulse will fully ionize the hydrogen (which becomes ionized near 2×10^{14} W/cm^2), and the hydrogen density and laser pulse duration are chosen to be nearly resonant such that a large amplitude wakefield (plasma wave) is generated. This wakefield has a velocity near the speed of light and is capable of accelerating electrons that are injected at the proper phase to high energies. The electron orbits in phase space (momentum versus longitudinal phase $z - ct$) are separated into two distinct regions, namely, trapped and untrapped orbits, by a critical orbit known as the separatrix.[27] Electrons from the ionized hydrogen lie essentially on the cold fluid orbit, i.e., untrapped orbits that constitute the plasma wave oscillation. However, electrons that are ionized near the peak of the laser pulse can be born (i.e., injected essentially at rest) at the proper phase such that they reside above the wake separatrix and, therefore, are trapped and accelerated. This is the case for inner shell electrons of a high Z atom, which have an ionization potential that corresponds to the peak intensity of the laser pulse. This is illustrated schematically in Fig. 1. In the following, we analyze this process, including determination of the appropriate high Z gas and calculation of the threshold laser intensity required for ionization injection.

In addition, we examine the use of a "two-stage" gas structure to control the injection process. The "two-stage" gas structure consists of an initially short section of a low concentration of high-Z gas (for injection into the plasma wave) followed by a long section of pure low-Z gas for post-acceleration without additional trapping or dark current (see Fig. 2). Following a short ionization injection section by a long acceleration section allows for the generating of electron bunches with low energy spread. The effects of gas composition, concentration, and length of the high Z gas region on the number of injected (i.e., trapped) electrons and on the final electron beam quality are studied. Laser pulse shape, polarization, and intensity effects on the final beam emittance are also studied. With proper injection parameters, mono-energetic electron beams, with 10 pC charge, can be generated in a mixed gas with ionized electron density of 10^{18} cm^{-3}.

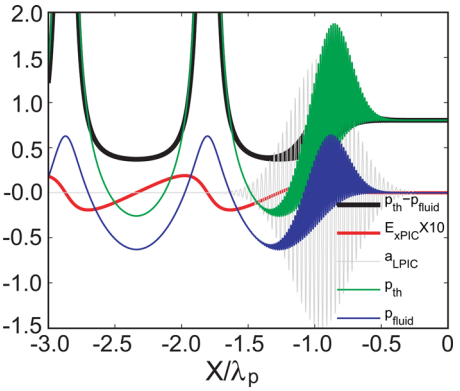

FIG. 1. (Color online) Typical laser plasma accelerator structure and injection scheme. The light black line shows a laser electric field distribution along its propagation direction. The thick red/gray line shows the electric field of the wake. The thin blue/dark gray line shows the momentum distribution of the background electron fluid. The thin green/gray line shows the trapping momentum threshold of the electrons in the wakefield. The thick black line shows the momentum gap between the trapping threshold and the background electron's momentum. Here, $a_0 = 1.5, L_{\mathrm{FWHM}} = 0.353\lambda_p$ (where λ_p is the plasma wavelength), and $n_e = 0.001 n_c$.

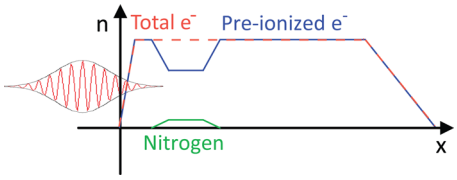

FIG. 2. (Color online) Schematic profile of the gas density distribution. The density of the pre-ionized electrons (n_e) and the neutral nitrogen atomic density (n_{N}) satisfy $n_e(x) + 5n_{\mathrm{N}}(x) = constant$. So the total density of the pre-ionized electrons and the electrons from ionization up to the 5th level of the nitrogen is uniform ($0.001 n_c$).

This paper is organized as follows. Section II presents a Hamiltonian analysis of the electron dynamics and the ionization-induced trapping condition is derived. Section III discusses the selection of the high-Z gas for ionization trapping. Section IV presents one- and two-dimensional particle-in-cell (PIC) simulations of the ionization injection. Asymmetric laser pulse profiles are considered in Sec. IV C to improve the quality of the trapped electron beam. The effect of laser polarization is discussed in Sec. IV E. Conclusions are offered in Sec. V.

II. ELECTRON DYNAMICS AND TRAPPING PHYSICS

In this section, we discuss the dynamics of electrons ionized in the plasma wave. We assume tunneling photoionization (see Appendix A) for the production of free electrons by the laser field, and the electrons are assumed to be ionized at rest. In the injection region, we consider a small concentration of high-Z gas mixed with pure H. For simplicity, since we are considering a small concentration of high-Z gas, we will neglect the modification of the wakefield due to the ionization process. This effect is considered in Appendix B.

The dynamics of a single test electron in a nonlinear plasma wave is determined by the potential of the plasma wave. In one-dimension, the electron motion in the plasma wave is described by the Hamiltonian[27] $H(\gamma, \psi) = \gamma - \gamma\beta\beta_p - \phi(\psi)$ or

$$H(u, \psi) = (\gamma_\perp^2 + u^2)^{1/2} - \beta_p u - \phi(\psi), \tag{1}$$

where $\gamma = (\gamma_\perp^2 + u^2)^{1/2}$ is the Lorentz factor of the electron, β is the longitudinal velocity normalized to c, $u = \gamma\beta$ is the normalized longitudinal momentum, $\beta_p \simeq 1 - \omega_p^2/2\omega_0^2$ is the normalized phase velocity of the plasma wave, $\psi = k_p\xi = k_p(x - \beta_p t)$ is the plasma wave phase with $k_p^2 = 4\pi e^2 n_0/m_e c^2$, and $\phi = e\Phi/m_e c^2$ is the electrostatic potential of the plasma wave normalized to the electronic rest energy. Here, $\gamma_\perp = (1 + u_\perp^2)^{1/2}$ is the transverse Lorentz factor and $u_\perp$ is the normalized transverse momentum of the electron.

Along an electron orbit $H=$constant, the particle momentum as a function of the Hamiltonian is

$$u = \beta_p\gamma_p^2(H+\phi) \pm \gamma_p[\gamma_p^2(H+\phi)^2 - \gamma_\perp^2]^{1/2}. \quad (2)$$

The separatrix orbit defining trapped and untrapped orbits is given by $H(\gamma_s,\psi) = H(\gamma_p,\psi_{\min})$, where $\phi(\psi_{\min}) = \phi_{\min}$, i.e.,

$$H_s = \gamma_\perp(\psi_{\min})/\gamma_p - \phi_{\min}. \quad (3)$$

An electron will be in a trapped orbit provided $H \le H_s$. For an electron initially at rest before the laser, $H=1$. For an initially warm plasma, $H = H_t \simeq 1-\beta_p u_t$, where $u_t \ll 1$ is the initial (non-relativistic) thermal momentum. For example, for a thermal plasma[28] behind the drive laser, trapping occurs for $1-\beta_p u_t \simeq H_t \le H_s = \gamma_p^{-1} - \phi_{\min}$ or $\phi_{\min} \le -1+\gamma_p^{-1}+\beta_p u_t$.

For an electron ionized inside the laser pulse in the 1D limit, the transverse canonical momentum is conserved $\partial_\psi(\boldsymbol{u}_\perp\text{-}\boldsymbol{a}_\perp)=0$. For an electron ionized at a wake phase ψ_i,

$$\boldsymbol{u}_\perp(\psi) = \boldsymbol{a}_\perp(\psi) - \boldsymbol{a}_\perp(\psi_i), \quad (4)$$

where we have assumed that the electron is born at rest, i.e., $u_\perp(\psi_i) = 0$. Note that if the electron is ionized at the peak of the laser electric field, then $a_\perp(\psi_i) = 0$. However, some electrons will be ionized off-peak with finite $a_\perp(\psi_i)$. The Hamiltonian of the ionized electron is

$$H_i = \gamma_\perp(\psi_i) - \phi(\psi_i) = 1 - \phi(\psi_i). \quad (5)$$

For the ionized electron to be trapped requires

$$H_i = 1-\phi(\psi_i) \le H_s = \gamma_\perp(\psi_{\min})/\gamma_p - \phi_{\min}. \quad (6)$$

Once the ionized electron leaves the laser field, $\gamma_\perp = (1+u_\perp^2)^{1/2} = (1+a_\perp^2(\psi_i))^{1/2}$. Therefore, the condition on the initial ionization phase for trapping is

$$1+\phi_{\min} - \phi(\psi_i) \le (1+a_\perp^2(\psi_i))^{1/2}/\gamma_p, \quad (7)$$

which assumes that the electron becomes trapped behind the laser pulse, i.e., $a_\perp(\psi_{\min}) = 0$. This trapping condition includes the effect of the residual transverse momentum that results from the electron being born inside the laser pulse, i.e., $\gamma_\perp = (1+a_\perp^2(\psi_i))^{1/2}$. This is equivalent to the condition given in Ref. 25.

The above trapping condition relates the phase at which the electron was ionized ψ_i to the minimum potential $\phi_{\min}$ of the wakefield excited behind the laser pulse. The minimum potential $\phi_{\min}$ can be related to the maximum electric field of the wake $E_{\max}$ and the laser pulse amplitude a_0 by considering the cold plasma fluid response. Neglecting the small modification to the wakefield owing to the production of additional plasma in the laser pulse via ionization (cf. Appendix B), the quasi-static laser-driven plasma wave equation is

$$\frac{\partial^2\phi}{\partial\psi^2} = \gamma_p^2\left\{\beta_p\left[1-\frac{\gamma_{\perp f}^2}{\gamma_p^2(1+\phi)^2}\right]^{-1/2} - 1\right\}, \quad (8)$$

where $\gamma_{\perp f} = (1+a_\perp^2)^{1/2}$ is the transverse Lorentz factor of the plasma fluid and $a^2 = 3.6\times10^{-19}(\lambda[\mu\text{m}])^2 I_0[\text{W/cm}^2]$, assuming circular polarization, where λ is the laser wavelength and I the laser intensity.

Behind the laser, the electrostatic potential oscillates between $\phi_{\min} \le \phi \le \phi_{\max}$, and the axial electric field oscillates between $-E_{\max} \le E \le E_{\max}$. The values $\phi_{\min}$ and $\phi_{\max}$, denoted by ϕ_m, are

$$\phi_m = \hat{E}_{\max}^2/2 \pm \beta_p[(1+\hat{E}_{\max}^2/2)^2 - 1]^{1/2}, \quad (9)$$

where $\hat{E}_{\max} = E_{\max}/E_0$ and the $\pm$ give $\phi_{\max}$ and $\phi_{\min}$, respectively. In the linear regime $\hat{E}_{\max} \ll 1$, $\phi_m = \pm\beta_p\hat{E}_{\max}$. In the nonlinear regime $\hat{E}_{\max} \gg 1$,

$$\phi_{\min} \simeq \left(-1+\frac{1}{2\gamma_p^2}\right)(1-\hat{E}_{\max}^{-2}) + \frac{\hat{E}_{\max}^2}{4\gamma_p^2}, \quad (10)$$

and, in the limit $\gamma_p \gg 1$, $\phi_{\min} \simeq -1+\hat{E}_{\max}^{-2}$. Hence, in the limits $\gamma_p \gg 1$ and $\hat{E}_{\max}^2 \gg 1$, the condition reduces to

$$\phi(\psi_i) \ge 1/\hat{E}_{\max}^2. \quad (11)$$

As an example, consider a weakly relativistic ($a_0^2 < 1$), linearly polarized, resonant sine-pulse laser with peak amplitude a_0. Within ($-2\pi \le \psi \le 0$) the laser pulse,

$$\phi = (a_0^2/8)[1-cos(\psi) - (\psi/2)sin(\psi)], \quad (12)$$

and behind ($\psi \le -2\pi$) the laser pulse, $\phi_{\min} = -\pi a_0^2/8$. The potential at the peak of the laser is $\phi(\psi=-\pi) = a_0^2/4$. Therefore, the minimum laser intensity for trapping is given by

$$1-\gamma_p^{-1} \le \phi(\psi_i) - \phi_{\min} \le (\pi/8+1/4)a_0^2 \simeq 0.64a_0^2. \quad (13)$$

For typical laser wakefield acceleration, where $\gamma_p > 10$, the above inequality cannot be satisfied for $a_0^2 < 1$. This indicates that the laser intensity must be relativistic ($a_0^2 > 1$) for ionization-induced trapping, which requires a fully nonlinear analysis.

In general, the trapping condition Eq. (6) can be evaluated for any excited plasma wave by solving the wake equation (8) for an arbitrary laser profile. Figure 3(a) shows the peak laser amplitude a_0 required for trapping versus the phase where the electron was ionized ψ_i. Figure 3(a) assumes excitation by a resonant (with rms intensity length $k_pL_{\text{rms}} = 1$) Gaussian laser pulse with intensity profile $a = a_0 exp[-\psi^2/4(k_pL_{\text{rms}})^2]$ and $\gamma_p = 33$. Electrons are assumed ionized at a phase peak of the electric field such that $a(\psi_i) = 0$. For electrons to be trapped at or in front of the peak of the laser envelope (at $\psi_i \ge 0$), the intensity must be $a_0 \ge 1.7$. Note that any trapping behind the peak of the laser pulse ($\psi_i < 0$) will be minimal, since the ionization rate is maximum at the maximum laser intensity; hence, the majority of ionization will occur at or before the peak of the laser pulse. Figure 3(b) shows the threshold laser intensity required to trap the ionized electrons at the peak of the laser envelope ($\psi = 0$) versus laser pulse length k_pL_{rms}.

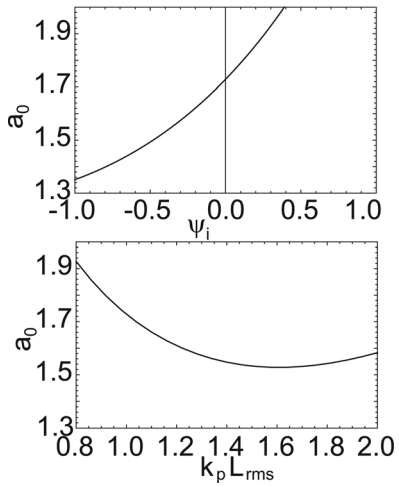

FIG. 3. (a) Threshold laser intensity a_0 required to trap an electron that was ionized at a phase ψ_i for a Gaussian laser centered at $\psi = 0$ with $k_p L_{\rm rms} = 1$ and $\gamma_p = 33$. (b) Threshold laser intensity a_0 required to trap at peak of laser envelope $\psi = 0$ versus laser pulse length $k_p L_{\rm rms}$.

Figure 3(b) indicates that one may use laser pulses longer than that for optimal wake excitation to move the peak of the laser field to a more advantageous wake phase for trapping. This also indicates that using skewed laser pulses may be preferred, as discussed in Sec. IV C.

III. HIGH-Z GAS SELECTION

The analysis in Sec. II demonstrates that electrons ionized sufficiently behind the head (e.g., near the peak) of the laser can be trapped for a sufficiently large plasma wave. For ionization injection, the large atomic potentials associated with inner shell electrons of high Z atoms enable some electrons to remain bound until the atom reaches a position near the peak of the laser field. Hence, when selecting an appropriate gas, the atomic potential for an inner shell electron should be high enough to bind the electron until reaching the proper phase for trapping, but not too high, such that the ionization rate is too low. Nitrogen is a good candidate for ionization-triggered injection from both theoretical and experimental considerations, since it is readily obtainable and has a large gap between the potential for the N^{5+} electron (97.9 eV) and the N^{6+} electron (552 eV). Consider a 0.8 μm wavelength laser operating at a normalized intensity of the order of $a_0 \sim 2$, i.e., a peak laser field of $E_{L0} \sim 8$ TV/m. From Appendix A, we see from the argument of the exponential function in Eq. (A1) that the ionization rate becomes significant for a peak laser field $E_{L0} \sim E_{ion}$, where $E_{ion} = (2/3)E_A(U_{ion}/U_H)^{3/2}$, with $E_A = 5.1$ GV/cm, $U_H = 13.6$ eV the ionization potential of hydrogen, and U_{ion} the ionization potential for given inner shell electron. For the N^{6+} electron, $U_{ion} = 552$ eV and $E_{ion} \sim 0.879$ TV/m; hence, a laser pulse with $a_0 = 2$ should be sufficient to readily ionize this state.

The precise amounts of ionization are given in Fig. 4, which shows the percentage of Nitrogen ionized for the transitions $N^{4+} \rightarrow N^{5+}$ (dashed black curve) and $N^{5+} \rightarrow N^{6+}$ (solid black curve), for a Gaussian laser pulse with $a_0 = 2$, $L_{\rm FWHM} = 14.89\lambda_0$, and $\lambda_0 = 0.8\mu$m. The light blue/gray curve shows the laser field, the blue/up dark gray curve shows the wakefield potential, the red/lower gray curve shows the electric field of the wake, and the ionization degree is shown by the black curve. Tunneling photoionization was considered, and the rate for ionization is described in Appendix A. For each point, $H_s - H$ is shown (green/middle gray curve) which depends on the wakefield ϕ. Trapping occurs for $H_s - H > 0$. Figure 4 shows that for the electrons ionized from $N^{4+} \rightarrow N^{5+}$, ionization occurs at the head of the laser pulse, where trapping condition is not satisfied. The electrons coming from the outer five electrons of nitrogen cannot be trapped in the wake. For the inner electrons $N^{5+} \rightarrow N^{6+}$, due to higher ionization potential, ionization has moved to near the peak of the laser pulse where $H_s - H > 0$ and electron trapping occurs. The laser intensity is not sufficiently high to cause significant ionization of $N^{6+} \rightarrow N^{7+}$.

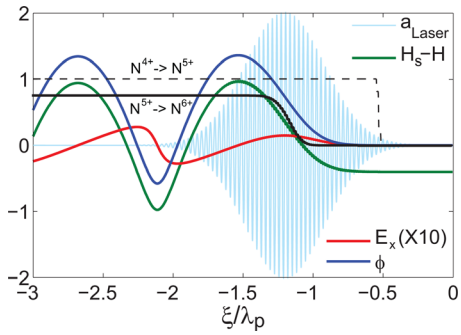

FIG. 4. (Color online) Normalized laser vector potential (light blue/gray curve), wake potential (blue/up dark gray curve), wake electric field (red/lower gray curve), $H_s - H$ (green/middle gray curve), and degree of ionization versus ξ/λ_p. The dashed black curve shows the degree of ionization for $N^{4+} \rightarrow N^{5+}$, and the solid black curve shows $N^{5+} \rightarrow N^{6+}$. Here, $a_0 = 2.0, L_{\rm FWHM} = 14.89\lambda_0$ (where λ_0 is the laser wavelength), and $n_e = 0.001 n_c$.

IV. PARTICLE-IN-CELL SIMULATIONS

The ionization-induced trapping mechanism was examined with PIC simulations using VLPL code[31] with photoionization. As discussed above, we consider a mixed gas of Hydrogen and Nitrogen. In the simulations, computational savings were realized by using electrons (instead of hydrogen atoms) and neutral nitrogen gas, i.e., the hydrogen was assumed fully ionized early in the laser-plasma interaction. As we can see in Appendix B, this kind of approximation is reasonable, since the hydrogen is ionized very quickly (i.e., at low intensity) and far before the laser peak and its ionization effect on the wake generation are negligible. The Ammosov-Delone-Krainov (ADK) tunneling ionization mechanism[32,33] was applied at every simulation step to check the ionization of the nitrogen ions. Laser energy loss due to ionization has been neglected since in our typical simulation it is only about 1.0×10^{-6} of the total laser energy. The density profile of the electrons and nitrogen gas is shown in Fig. 2. A short region of gas mixture (nitrogen and pre-ionized hydrogen) near the start of the stage is used for electron injection, while the remainder of the stage uses pure (pre-ionized) hydrogen gas (free of trapping for parameters used). The initial electron density is set to be uniform inside the plasma, once 5 electrons of the nitrogen are ionized in

the mixed gas region. In this way, the density ramp effects are negligible. This was confirmed by using tagged particles in the PIC simulations, in which the tags show the trapped electrons only come from the ionized electrons and no pre-ionized electrons in the ramp region have been trapped.

A. Maximizing trapped charge

A successful method for injection requires control over the number of injected electrons and the beam quality. For ionization-triggered injection, the beam quality and charge depend on the laser and gas parameters. In this section, we examine the effect of the length of the mixed gas region. To exclude the effects due to background plasma density gradients, in these simulations, we fix the total ionized (until the 5th electron of nitrogen, N^{5+}) electron density to be $n_H + 5n_{N^{5+}} = 0.001n_c$ with $n_c = 1.7 \times 10^{21}\text{cm}^{-3}$, the critical density for a laser of 800 nm wavelength, and vary the concentration of nitrogen at the mixed region to see the effect on the injection number. In the following one-dimensional (1D) simulations, the normalized laser electric field is $a_0 = 2.0$ and the FWHM of the pulse is $14.89T_0$, where T_0 is the laser period.

Figure 5(a) shows the relation between the injection number and the length of the mixed gas. Here, the concentration of nitrogen in the simulations is fixed to be $n_N/(n_N + n_H) = 1\%$ (red circle curve) or 2% (blue triangle). The injected number is counted for the electrons which satisfy

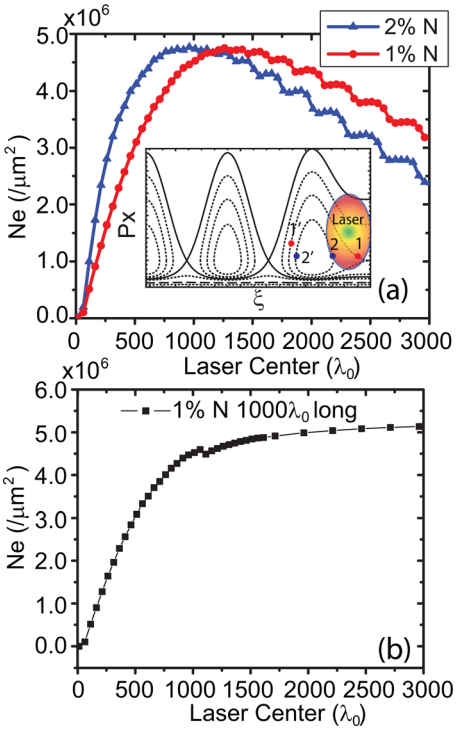

FIG. 5. (Color online) (a) Trapped electron number versus the laser propagation distance (position of the center of the laser pulse) in the mixed gas. Inset shows the electron orbits in longitudinal phase space: (1) orbits of an electron trapped near the separatrix (solid line) and (2) a deeply trapped electron. The laser pulse is represented by a colorful ellipse in the inset. (b) Trapped number evolution versus laser propagation distance. Here, the mixed gas length is fixed at $1000\lambda_0$. Laser-plasma parameters are $a_0 = 2.0, L_{\text{FWHM}} = 14.89T_0$, and a uniform plasma density $n_e = 0.001n_c$.

$H < H_s$, where ϕ is numerically calculated from the longitudinal electric field E_x in the PIC simulation. As Fig. 5(a) shows the injection number increases linearly with mixed gas length for short lengths. Fig. 5(a) also shows that a peak charge is reached (Q_s), followed by a decease in trapped charge versus mixed gas length. This is a beam loading effect. The field generated by the injected electron beam has canceled the laser generated wakefield and no electrons can be injected. In addition to saturating the amount of trapped charge, for longer mixed gas lengths, initially injected electrons are lost. This is due to the large injection volume in phase space [see inset of Fig. 5(a)]. Ionization injection allows electrons to be injected into deeply trapped orbits [e.g., orbit 2 of the inset of Fig. 5(a)]. This modifies the wakefield via beam loading allowing electrons trapped previously near the separatrix [e.g., orbit 1 of the inset of Fig. 5(a)] to be lost. Laser evolution may also reduce the wakefield amplitude and ionization rate. Note that the maximum trapped number Q_s is approximately equal for 1% and 2% concentration of the nitrogen with other parameters (laser and total ionized electron density) fixed, also due to the beam loading effect. The higher the nitrogen concentration the shorter the linear scaling region. The length of the linear region is $l_{\text{linear}} = Q_s/\kappa(a_0)\alpha_N$, where α_N is the Nitrogen concentration and $\kappa(a_0)$ is the ionization degree. This defines the slopes shown in the linear injection region in Fig. 5(a).

To avoid loss of trapped charge, one must limit the length of the mixed gas. Fig. 5(b) shows the injection number along the laser propagation position. The mixed gas length here is limited to $1000\lambda_0 = 800\mu$m. In this case, the injection process is terminated and the loss of trapped charge via beam loading is mitigated.

Although the maximum number of trapped electrons is reached by setting the length of the mixed gas to be just before beam loading saturates the charge, as we can see later, to achieve a high quality injection beam, a shorter mixed gas length is preferable. The longer the mixed gas region, the larger the phase difference between the newly ionized and trapped electrons and earlier trapped electrons. This spread in injection times broadens the electron beam energy spectrum. In addition, operating near the beam loading limit alters the wakefield, typically resulting in increased energy spread. The wakefield felt by the later trapped electrons is different from that felt by the initially trapped electrons owing to loading of the wakefield. A typical energy spectrum of an ionization-trapped electron beam with a long mixed gas length is shown in Fig. 6.

B. Gas length and concentration effect on beam quality

The mixed gas length has a strong effect on the obtainable minimum accelerated beam energy spread. Figure 7 shows the number (blue squares) and energy spread (black circles) of the injected electrons for different mixed gas lengths. The laser amplitude is $a_0 = 2.0$, and the nitrogen concentration is 1%. As seen in Fig. 7, when the gas length is $<1000\lambda_0$, the injected electron number is almost the same as the one we calculated from the potential method [cf.

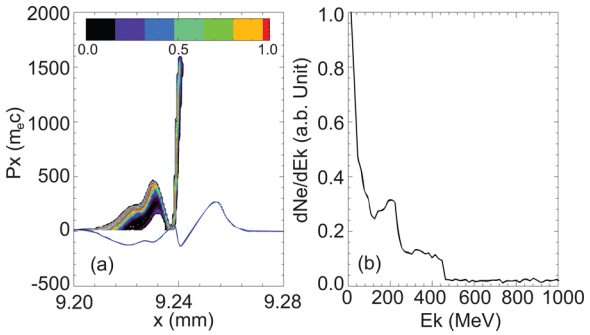

FIG. 6. (Color online) (a) Distribution of electrons in longitudinal phase space (x-p_x) and normalized electric field of the wake E_x (arbitrary units). The color bar represents the relative density in the phase space. (b) Electron energy spectrum (number versus electron energy E_k) beyond dephasing length. Laser pulse: $a_0 = 2.0$ and $L_{\mathrm{FWHM}} = 14.89T_0$. The uniform plasma density is $n_e = 0.001n_c$ with the full length being mixed gas (1% nitrogen).

Fig. 5(a)]. However, the beam energy spread is almost 60% when the mixed gas length is $1000\lambda_0$ (the mean energy of the beam is 1 GeV).

The energy spread has an approximately linear relationship with the mixed gas length for the laser-plasma parameters used in the simulation. The beam quality may be improved by reducing the gas length, but for fixed concentration, this will reduce the injected charge.

To get higher injection charge and beam quality, the concentration effect is studied as well. The trapped charge with a fixed mixed gas length depends on the nitrogen concentration. Figure 8 shows the injected electron number and beam energy spread versus nitrogen concentration, with the mixed gas length $200\lambda_0$ (the mean energy of the beam is 1 GeV). As shown in Fig. 8, when the concentration increases, both the injection number and energy spread increase. The injection number increases almost linearly, while the energy spread increases dramatically after a sufficiently high concentration (3% here) due to beam loading effects.

Both the concentration and mixed gas length affect the final beam energy spectrum; however, when the injection number is far lower than the saturation value Q_s, the mixed gas length effect is more important than the concentration effect. Figure 9 illustrates this dependence. In Fig. 9, we fix the product of concentration and mixed gas length. Since the injection

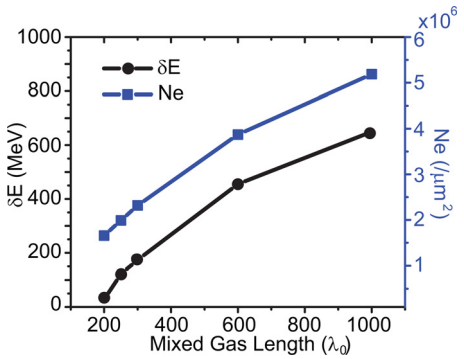

FIG. 7. (Color online) Electron beam energy spread (black circles) and injected electron number (blue squares) versus the mixed gas length. The laser-plasma parameters are $a_0 = 2.0, L_{\mathrm{FWHM}} = 14.89T_0$, and a uniform plasma density with $n_e = 0.001n_c$.

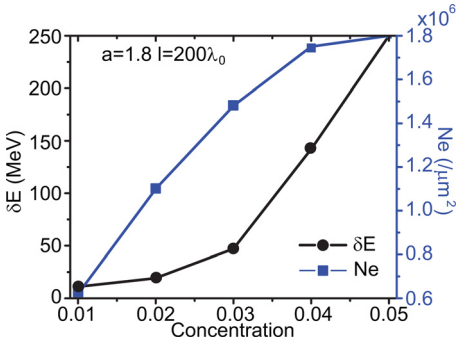

FIG. 8. (Color online) Dependence of energy spread and final electron injection number on the concentration of nitrogen. Here, the mixed gas length is $200\lambda_0$. Laser pulse: $a_0 = 1.8$ and $L_{\mathrm{FWHM}} = 14.89T_0$. The uniform plasma density is $n_e = 0.001n_c$.

number is in the linear regime, the final amount of trapped charge is approximately equal. However, the final beam energy spread linearly increases with the mixed gas length.

The minimum energy spread can be determined from the intercept of the curve (gas length tends to 0), which for this case is about 2.9 MeV on a final beam energy of 1 GeV. Two typical energy spectrums are shown in Fig. 9(b) corresponding to the two points in Fig. 9(a). A shorter mixed gas length improves the final beam energy spread. The results show that a shorter mixed gas length and higher concentration of mixed gas give a better accelerated beam. However, the minimum energy spread cannot be further reduced by shortening the mixed gas length. As we will see in the following, it is determined by the ionization process and can be improved by laser pulse shaping.

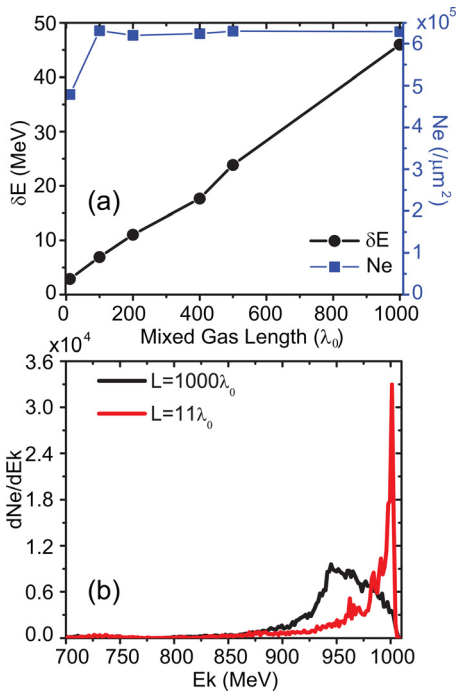

FIG. 9. (Color online) (a) Dependence of energy spread and final electron injection number on the mixed gas length. Here, the product of mixed gas length (unit in λ_0) and concentration (percentage) is fixed to be 2. (b) Electron energy spectrum when the mixed gas length is 1000 λ_0 long (black line) or 11 λ_0 long (red/gray line). Laser pulse: $a_0 = 1.8, L_{\mathrm{FWHM}} = 14.89T_0$, and the uniform plasma density $n_e = 0.001n_c$.

C. Laser pulse shape effect on beam quality

To identify the source of the energy spread, we examine the effects of the ionization phase (ξ_i) on the trapped electrons. Here, ξ_i is the phase at which the electron was initially born. Figures 10(a) and 10(b) shows the distribution of the electron longitudinal momenta versus the ionization phase ($\xi_i - \xi_{\text{laserpeak}}$) at times (a) $t = 800$ and (b) $t = 1600$. It shows that two components contribute to the final energy spectrum: (1) ionization at a fixed ξ_i occurring throughout the entire length of the mixed gas region, and (2) the spread in ionization phases of the trapped electrons. For the electrons that have the same value of ξ_i, the trajectory in phase space is the same. (Here, we assume the beam loading effect is negligible.) However, due to the different ionization positions (or time) in the lab frame, the electrons arrive at the peak energy at different times. This gives the slice energy spread shown in Fig. 10(a) and is determined by the mixed gas length.

The other energy spread source comes from the distribution of different ionization phases. Due to the probabilistic nature of the ionization process (see Appendix A), electrons ionized at the same position in the plasma can be born at different phases with respect to the laser pulse (and wakefield). The tunneling ionization rate is maximum at the maximum electric field of the laser pulse. For a realistic laser pulse with length $\gg \lambda_0$, ionization will not be localized to a single phase peak of the electric field, but will be spread over several neighboring phase peaks with comparable values of electric field amplitudes. This constitutes an intrinsic energy spread for the ionization injection process. These electrons will have different trajectories in the phase space, and the energy gain will be determined by the ionization phase. If we reduce the length of the mixed gas, the energy spread due to the first process can be reduced. However, the tunneling photo-ionization mechanism will still generate an energy spread. To minimize the energy spread, one can select a gas composition for which the peak laser intensity is very close to the ionization threshold of the trapped valence electron in combination with using an ultrashort laser pulse (i.e., limit the phase region where ionization is probable).

Another option for reducing the energy spread is to shape the laser pulse to ionize at preferred phases of the wakefield. To illustrate the effect of laser pulse shaping, we consider the case of a skewed laser pulse with temporal profile,

$$a(t) = a_0 exp\left[-\frac{t^2}{\tau^2}\frac{1}{1 + bt/\sqrt{t^2 + (\tau/2)^2}}\right], \qquad (14)$$

where b is the skew parameter. For $b = 0$, the pulse profile is Gaussian with $L_{FWHM} = \sqrt{2ln2}\tau$. In the following simulations, $a_0 = 1.8$ and $L_{FWHM} = 14.89T_0$. Figure 11(a) shows the transverse field of the laser and the electric field of the wake for a skewed laser profile with $b = -0.8$. For a negatively skewed laser pulse profile, ionization occurs more deeply into the wakefield where the wake potential is larger. This reduces the volume of the electrons in phase space and improves the energy spread. Figure 11(b) shows the electron energy spectrum produced by positively ($b = 0.8$) and negatively ($b = -0.8$) skewed lasers. Here, we compare the spectrum at the same maximum electron energy and before the dephasing length is reached to illustrate the effect of the distribution in ionization phases. The positively skewed pulse gives a larger energy spread compared to the negatively skewed pulse. Note that the example show in Fig. 11 is not optimized, but illustrates the potential improvements by using shaped laser pulses. Previously skewed lasers have been employed to seed the laser self-modulational instability.[34,35]

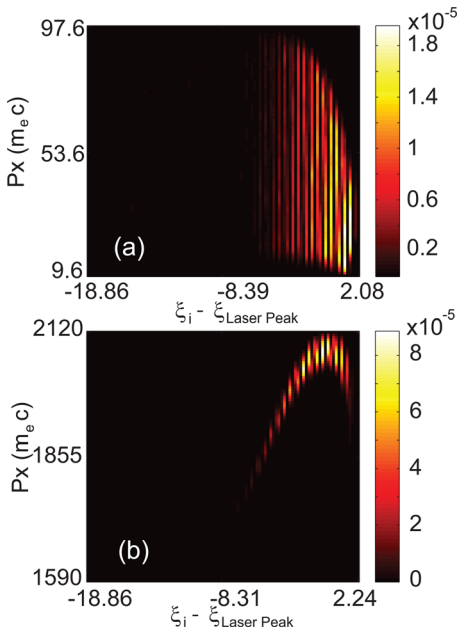

FIG. 10. (Color online) Electron momentum distribution versus initial ionization phase with respect to laser peak $\xi_i - \xi_{\text{laserpeak}}$ for (a) $t = 800T_0$ and (b) $t = 1600T_0$.

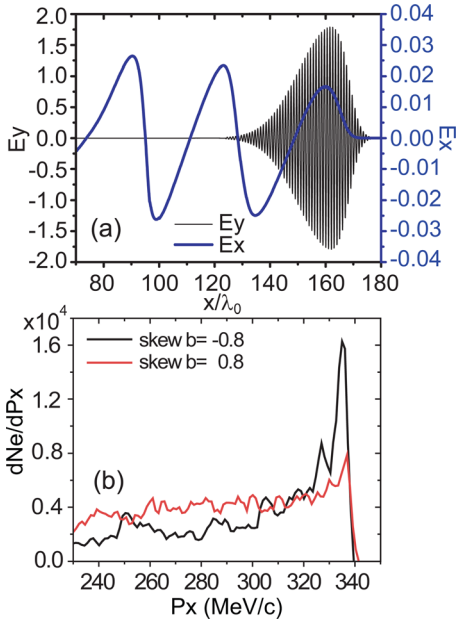

FIG. 11. (Color online) (a) Skewed ($b = -0.8$) laser pulse transverse field (thin black) and excited wakefield (thick blue/dark gray) normalized by $m_e\omega_0 c/e$. (b) Electron beam energy spectra using a laser with a positive (red/gray) and negative skew (black).

D. Transverse emittance from ionization

Small beam transverse emittance is critical to many applications. In the case of ionization injection, contributing to the initial transverse emittance is the residual transverse momentum from the ionization process. Although the ADK model predicts that the electrons are preferentially ionized at the peak of the electric field, where the laser vector potential is zero, the tunneling process allows electrons to be ionized off-peak at a phase such that the laser vector potential is non-zero. For a circularly polarized laser pulse, it is always used to reduce the energy spread of the injected electrons[29] due to the lower electric field intensity closed to the ionization threshold. However, the laser vector potential is always nonzero at all ionization positions. The finite vector potential at the ionization time will result in a finite transverse momentum after leaving the laser, which will contribute to the final beam transverse emittance.[30] This phenomena has been demonstrated using 1D-PIC simulations as shown in Figs. 12(a) and 12(b).

To minimize the effect of electrons obtaining transverse momentum from being ionized off-peak of the laser electric field, one could consider tuning the laser parameters and gas selection to allow for ionization only near the peak intensity of the laser pulse. Fig. 12(c) shows the final injection number and transverse momentum of the electrons versus laser intensity. A lower laser intensity gives smaller residual transverse momentum; however, fewer electrons are trapped. To compensate for this low trapping number, one could increase the gas concentration to increase the trapping number.

E. Multi-dimensional and laser polarization effects

In this section, we examine multi-dimensional effects on ionization-induced trapping using two-dimensional PIC simulations. The multi-dimensional trajectories of the electrons trapped from ionization differ strongly from those self-injected in the bubble regime without ionization.[36,37]

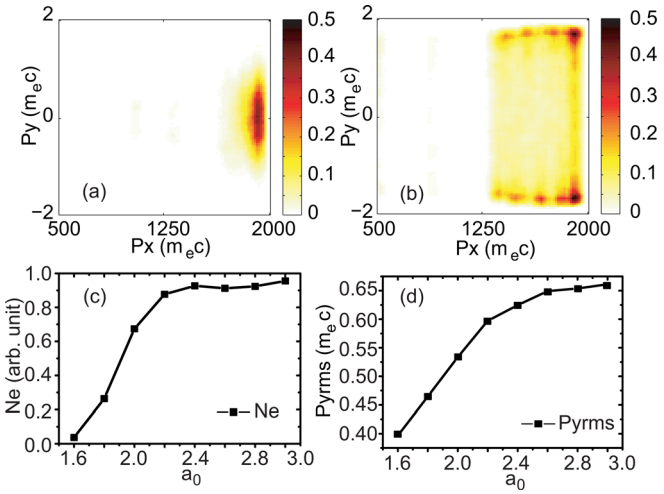

FIG. 12. (Color online) Transverse momentum distribution of trapped electrons using a laser with (a) linear polarization or (b) circular polarization. The laser-plasma parameters are $a_0 = 2.0, L_{\mathrm{FWHM}} = 14.89T_0$, and the plasma density $n_e = 0.001n_c$. (c) Number of trapped electrons and (d) transverse momentum (root mean square) versus a_0 using a linearly polarized laser pulse.

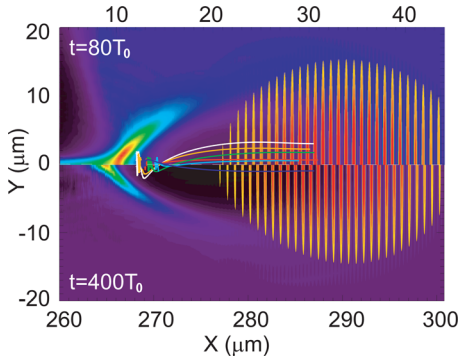

FIG. 13. (Color online) Typical trajectories of trapped electrons via ionization. Laser-plasma parameters are $a_0 = 2.0, L_{\mathrm{FWHM}} = 14.89T_0$, focus spot size $W_{\mathrm{FWHM}} = 17.66\lambda_0$, uniform plasma density with $n_e = 0.001n_c$, and mixed gas length $l = 20\lambda_0$. The nitrogen concentration is 1%. Top half shows $t = 80T_0$ and bottom half shows $t = 400T_0$.

Figure 13 shows typical trajectories of electrons trapped via ionization injection. Note that trapped electron trajectories move through the interior of the bubble, rather than along the bubble sheath as in self-injection. The trapped electrons do not originate within a small transverse region off-axis, as in the case of self-injection, but from a wide distribution in the transverse direction. One possible consequence of this is a wider spectrum of emitted synchrotron radiation.[38]

We now examine the effect of laser polarization and consider two cases: laser polarization perpendicular to the plane of the simulation box (S-polarization or out-of-plane polarization) and laser polarization parallel in the plane of the simulation box (P-polarization or in-plane polarization). The spatial distribution of trapped electrons for S-polarization and P-polarization are shown in Figs. 14(a) and 14(b), respectively. For the case of S-polarization the electron distribution exhibits a filamented structure in the simulation plane. Early during acceleration, these filaments periodically merge and re-form, and then disappear at later times for high beam energy. For the case of P-polarization, we do not observe such kinds of structures throughout the

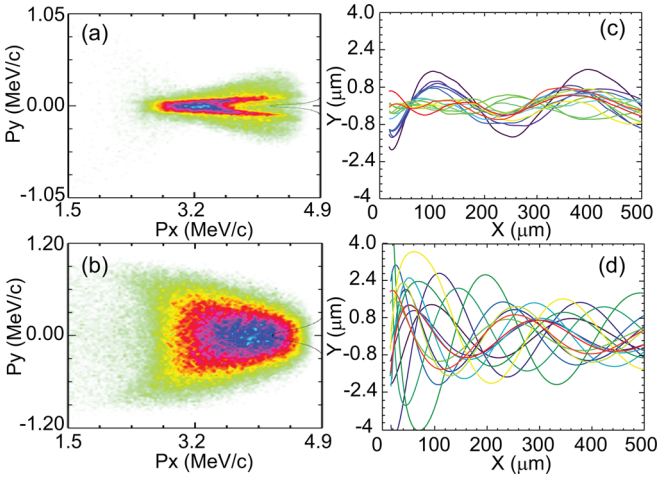

FIG. 14. (Color online) Transverse spatial structure of the accelerated electron beam using (a) S-polarized laser pulse and (b) P-polarized laser pulse when $t = 120T_0$. Typical trajectories of trapped electrons for the (c) S-polarized and (d) P-polarized cases, respectively. Except polarization, other laser and plasma parameters are the same as in Fig. 13.

simulation. Typical trapped electron trajectories for the cases of S-polarization and P-polarization are shown in Figs. 14(c) and 14(d), respectively. For the case of S-polarization, the trajectories are undergoing semi-coherent betatron oscillations in phase with period $\lambda_\beta \sim \sqrt{2\gamma}\lambda_p$. The energy spread of the electrons provides for mixing of the betatron oscillations, eliminating the filaments at later times. For the case of P-polarization, the electron trajectories are out of phase (primarily incoherent). This is a result of the residual transverse momentum obtained from the tunneling ionization process. Correspondingly, the spatial distribution is more uniform and the transverse momentum spread is larger [cf. Fig. 14(b)]. We think in the 3D geometry the initial beam structure inside the wake will be an axis asymmetric structure. In the transverse direction parallel to the laser electric field, the beam will have a Gaussian distribution; however, in the vertical plane, the beam will have bifurcation structures and later will be mixed into a Gaussian distribution.

The simulation results show the injected electron number is similar between the two polarization cases ($9.92 \times 10^5/\mu$m for P polarization case and $1.06 \times 10^6/\mu$m for S polarization case). After the laser propagation length of 508μm, the center beam of the P polarization case is 50.2 MeV, which is a little larger than the S polarization case (48.89 MeV) due to the smaller beam loading effect. The energy spread in the S polarization case is $\delta E_{FWHM} = 1.58$ MeV. In the P polarization case, it is $\delta E_{FWHM} = 2.15$ MeV. The root-mean-square (rms) energy spread of the two cases are similar ($\delta E_{rms} = 7.71$MeV for P polarization and $\delta E_{rms} = 7.38$MeV for S polarization). For the circular polarization case, we use the same laser amplitude $a_0 = 2.0$ which is used for the transverse momentum spread comparison with the linear polarization case as we talked before in Fig. 12. With this intensity, both the ionization degree and wakefield structure are quite different. The final injected electron number is $5.91 \times 10^6/\mu$m, and the center energy is 30.35 MeV with an energy spread of $\delta E_{FWHM} = 14.04$MeV and $\delta E_{rms} = 34.17$MeV.

We also performed a 1D simulation with these parameters for a linearly polarized laser pulse for comparison. The results show the final injected electron number is about $1.64 \times 10^5/(\mu m)^2$. Compared with the 2D simulation results, this implies that the effective transverse injection size is about 6.46μm, which is far less than the laser width 14.13μm. The laser amplitude at $r_\perp = 3.2\mu$m is $a = 1.86$, which is far above the threshold for the ionization injection. The reason for the non-trapping of the electrons ionized beyond the transverse region is transverse loss. The electrons ionized there will not only feel the longitudinal acceleration, but also the transverse forces, and some electrons will transversely pass through the wake and will not be trapped. The accelerated beam energy is similar in all of the cases. The 1D simulation gives a center energy of 46.65 MeV and an energy spread of $\delta E_{FWHM} = 2.59$MeV.

V. CONCLUSION

We have theoretically examined the ionization injection process by a single laser pulse in a laser-plasma accelerator. In order to improve the beam quality and to control the amount of trapped charge, we considered a short segment of mixed gas, containing a high-Z gas component (e.g., nitrogen), for injection followed by a longer segment of hydrogen gas for post-acceleration. The effects of gas composition, mixed gas segment length, and concentration on the final electron beam quality were studied.

Ionization injection requires that the laser intensity and gas selection satisfy two criteria. (1) The laser intensity needs to be sufficiently high in order to generate a sufficiently large wakefield such that if an electron was born at rest near the peak intensity of the laser pulse, then it would lie above the wake separatrix and become trapped; (2) An appropriate high Z gas must be selected such that the ionization threshold for an inner shell electron corresponds very closely to the peak intensity of the laser pulse. Using 1D theory, it was shown that the minimum laser amplitude required to trap an electron ionized at the peak of the laser pulse is $a_{min} \simeq 1.7$, assuming a resonant Gaussian laser pulse with $k_p L_{rms} = 1$. By using a somewhat longer laser pulse $k_p L_{rms} \simeq 1.5$, or by using a skewed pulse, this threshold can be reduced to $a_{min} \simeq 1.5$. An appropriate choice of gas for ionization injection at this laser amplitude (assuming a 0.8 μm laser) is nitrogen, which has an ionization potential of 552 eV for the N^{5+} electron.

For fixed laser parameters, the amount of trapped charge from ionization injection depends on the concentration of the high Z gas and the length of the mixed gas region. It was shown that the beam loading effect will limit injection and also increase the energy spread. To avoid increased energy spread, it is essential to limit the length of the mixed gas region as well as the concentration of the high Z gas such that the total trapped charge is sufficiently below the beam loading limit. In this regime, the total trapped charge is determined by the product of the mixed gas length and the concentration of the high Z gas.

The beam energy spread for cases below the beam loading limit is primarily from two sources: a spread in trapping times (i.e., different acceleration lengths) and a spread in injection phases (i.e., different trajectories in phase space). By proper selection of gas composition or by using laser pulse shaping, the ionization distribution in the wake phase space may be controlled and the final energy spread reduced. A short mixed gas region is essential to reducing the spread in injection times and minimizing the spread in the acceleration length, and hence, the spread in final energies. The use of two-stage (injector and accelerator) gas cell can be used to reduce the initial injection energy spread and reduce relative energy spread in further by later acceleration. This scheme has recently been successfully demonstrated by Pollock *et al.*, in which a 460 MeV electron beam with $<5\%$ energy spread is produced.[39] The energy spread can also be reduced by confining ionization to a small region within the laser pulse. This can be accomplished by selecting a high Z gas with an ionization potential that corresponds very closely to the peak laser intensity, in combination with using an ultrashort laser pulse.

The residual transverse electron momentum following ionization contributes to the final transverse emittance of the

acceleration beam. For circular polarization, ionization occurs at laser phases where both the electric field and the vector potential are maximum. Hence, the residual transverse momentum will be maximum $u_\perp \simeq a_0$. This will result in a large transverse momentum.[30] For these reasons, circular polarization should not be used when considering ionization injection. For linear polarization, the phase peaks in the electric field correspond to phases at which the vector potential is zero. Although ionization is maximum at the maximum electric field, some ionization will occur off-peak, which corresponds to the electrons being born at finite values of the vector potential and results in finite residual transverse momentum. Operating near the minimum intensity for ionization can reduce the residual transverse momentum. This effect, in combination with the transverse ponderomotive force of the laser, results in electrons injected with finite transverse momentum. This results in betatron motion and non-zero emittance. In the plane perpendicular to the laser polarization, the betatron motion is partially coherent, resulting in a filamented structure in phase space. In the plane parallel to the laser polarization, the residual transverse momentum facilitates betatron mixing and a more uniform structure in phase space.

Particle-in-cell simulations in 2D indicate that ionization injection can result in the production of high quality electron bunches for parameters that can be achieved in the laboratory in the near term. The example shown in Figs. 13 and 14 assume a laser of amplitude $a_0 = 2.0$, length $L_{\mathrm{FWHM}} = 39.8$ fs, and width $W_{\mathrm{FWHM}} = 14.13\mu$m interacting with a mixed gas with length 16μm. For these parameters, ionization injection results in the production of an electron bunch with a center energy of 84 MeV after a propagation length of 844μm. The beam energy spread is $\delta E_{\mathrm{FWHM}} = 1.78$ MeV, i.e., a normalized energy spread of $\delta E/E \simeq 2\%$, which is on the order of that observed in self-injection[5] and colliding pulse[16] experiments. The final injected electron number is $1.05 \times 10^6/\mu$m in the 2D slab geometry of the simulation.

Although in this work we have considered ionization injection using only a single pulse in detail, other geometries may be advantageous.[23] For example, two or more additional laser pulses propagating in the transverse direction with sufficient intensity to ionize may be used to trap electrons. In this geometry, the residual momentum will be in the forward direction, thereby reducing the transverse emittance. More complicated geometries using multiple pulses will be the subject of future work.

ACKNOWLEDGMENTS

The authors would like to thank Lule Yu, Carlo Benedetti, and Stepan Bulanov for useful discussions. This work was supported by the Director, Office of Science, Office of High Energy Physics, of the U.S. Department of Energy under Contract No. DE-AC02-05CH11231 and by the National Science Foundation under Grant No. PHY-0935197. Computational resources of the National Energy Research Scientific Computing Center were used to perform the simulations.

APPENDIX A: TUNNELING PHOTO-IONIZATION

In this Appendix, we review tunneling photo-ionization physics. The probability of tunneling ionization with an initial energy (ϵ) is given by[33,40]

$$w(\epsilon) \sim exp\left\{-\frac{2}{3}\left[\frac{\lambda_0}{\lambda_C}a^3\gamma_K^3\frac{E_k}{|E(\tau)|}+\frac{\gamma_K^3\epsilon}{\hbar\omega}\right]\right\}, \tag{A1}$$

where $E(\tau)$ is the field of the laser, $E_k = m_e c^2 k_0/e$, $\gamma_K = (U_i/2U_p)^{1/2} = (\alpha_f/a)(U_i/U_H)^{1/2}$ is the Keldysh parameter, with $U_H = 13.6$ eV the ionization potential of Hydrogen, U_i is the ionization potential, $U_p = m_e c^2 a^2/4$ is the laser ponderomotive potential, $\alpha_f = e^2/\hbar c \simeq 1/137$ is the fine structure constant, and $\lambda_C = h/m_e c = 2.4263 \times 10^{-10}$ cm is the Compton wavelength. In the high-field limit (long wavelength regime) $\gamma_K < 1$, tunneling ionization is dominant. In Eq. (A1), we have omitted the initial momentum along the laser transportation direction which is far less than the one along the laser polarization direction.[33] The form for the algebraic terms prior to the exponential in Eq. (A1) used in this paper is determined from the time-averaged AC tunneling ionization rate.[41] A comparison of the DC and AC tunneling ionization rates will be the subject of a future publication.

Note that Eq. (A1) indicates that the electrons will be mainly ionized at the peak of the laser electric field. This corresponds to a minimum of the laser vector potential, i.e., $\boldsymbol{E} = -c^{-1}\partial_t \boldsymbol{A}$. Because transverse canonical momentum will be approximately conserved, $\boldsymbol{p}_\perp \simeq e\boldsymbol{A}_\perp mc$, the electrons ionized at the peak of the laser field have zero transverse momentum upon exiting the laser, allowing them to be trapped in the longitudinal field of the plasma wave. Electrons ionized off-peak of the laser electric field exit the laser with a residual transverse momentum. As shown in Sec. IV D, this residual transverse momentum contributes to the transverse emittance.

As we can see from Eq. (A1), the initial energy spread of the electrons ionized by the laser field is about $\delta E_i \simeq 3\hbar\omega/2\gamma_K^3$. In our case, if we use the Keldysh parameter near the ionization point ($a \sim 1.5$) for N^{5+} ions, this gives $\delta E_i \simeq 0.433 m_e c^2$. This will add another intrinsic quantum energy spread and transverse emittance to the final accelerated beam. The precise results can be obtained by solving the time-dependent Schrödinger equation to get the correct ionization distribution; however, this was not done in the current PIC simulations due to the computational cost and time. For the outer 5 electrons of nitrogen, $\delta E_i \sim$ keV $\ll m_e c^2$, which is negligible and has been omitted in PIC simulation as well.

Figure 15 shows the spatial distribution of the ionization rate versus the laser vector potential and the position along the laser pulse. Here, we consider ionization such that $N^{5+} \rightarrow N^{6+}$, normalized laser intensity $a_0 = 2.0$, and length of $L_{\mathrm{FWHM}} = 14.89T_0$. Note that for nitrogen, the ionization potentials for N^{4+}, N^{5+}, N^{6+}, and N^{7+}, are 77.472 eV, 97.888 eV, 552.057 eV, and 667.029 eV, respectively.

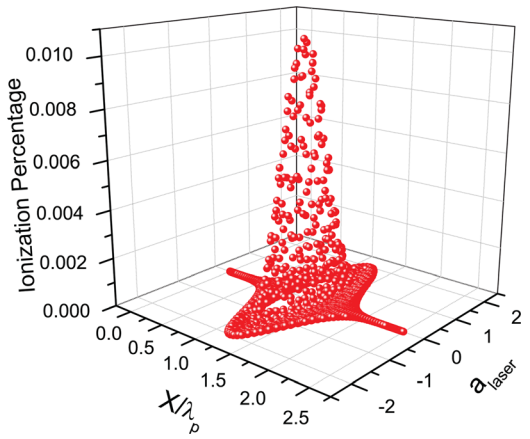

FIG. 15. (Color online) Distribution of ionization rate in the space of the laser vector potential and the position along the laser pulse. Here, the ionization $N^{5+} \rightarrow N^{6+}$ and normalized laser intensity $a_0 = 2.0$ and length of $L_{FWHM} = 14.89T_0$ are considered.

APPENDIX B: WAKEFIELD EXCITATION DURING PLASMA IONIZATION

In this appendix, we examine the effect of ionization on plasma wave excitation. Assuming the quasi-static approximation, the one-dimensional, cold plasma electron fluid has the following evolution equations:

$$\partial_\xi[n_e(1-\beta_x)] = \partial_\xi n_i, \tag{B1}$$

$$\partial_\xi[u_\perp - a_\perp] = \frac{-u_\perp}{n_e(1-\beta_x)}\partial_\xi n_i, \tag{B2}$$

$$\beta_x\partial_\xi u_x + \beta_\perp\partial_\xi a_\perp - \partial_\xi(u_x+\phi) = \frac{u_x}{n_e}\partial_\xi n_i, \tag{B3}$$

for the plasma density, transverse fluid momentum, and axial fluid momentum, respectively. Here, we assume fixed ions created via laser ionization and $\xi = x - ct$ is the co-moving variable. We will assume electrons are initially at rest upon ionization $\boldsymbol{u}(\xi_i) = 0$, where ξ_i is the ionization position in the laser. We will also assume instantaneous creation of photo-ionized electron-ion pairs,

$$n_i = H(\xi - \xi_i)n_0, \tag{B4}$$

such that $\partial_\xi n_i = \delta(\xi - \xi_i)n_0$. With this boundary condition and the initially cold electron plasma assumption, the equations of motion Eqs. (B1)–(B3) can be integrated to yield the constants of motion,

$$\gamma - u_x - \phi = 1 - \phi(\xi_i), \tag{B5}$$

$$u_\perp = a_\perp - a_\perp(\xi_i), \tag{B6}$$

$$n_e - n_i - n_e\beta_x = 0. \tag{B7}$$

Note that, if the assumption of instantaneous ionization Eq. (B4) or the initially cold assumption $\boldsymbol{u}(\xi_i) = 0$ is relaxed, then Eqs. (B5) and (B6) contain additional terms from the integration of Eqs. (B2) and (B3). Combining the constants of motion Eqs. (B5)–(B7) yields the equation of the electron density,

$$\frac{n_e}{n_i} = (1-\beta_x)^{-1} = \frac{1+[a_\perp - a_\perp(\xi_i)]^2 + [1-\phi(\xi_i)-\phi]^2}{2[1-\phi(\xi_i)-\phi]^2}. \tag{B8}$$

For simplicity, consider two species: one ionized at the head of the laser with ion density $n_{i1} = \alpha n_0$ and one ionized at ξ_i with ion density concentration $n_{i2} = (1-\alpha)H(\xi - \xi_i)n_0$. Here $\alpha < 1$, such that the electron plasma density following the laser is n_0. Using the Poisson equation, the evolution of the quasi-static laser-driven plasma wave is given by

$$\begin{aligned} k_{p0}^{-2}\frac{\partial^2\phi}{\partial\xi^2} &= \frac{n_{i1}}{n_0}\left(\frac{n_{e1}}{n_{i1}} - 1\right) + \frac{n_{i2}}{n_0}\left(\frac{n_{e2}}{n_{i2}} - 1\right) \\ &= \frac{\alpha}{2}\left[\frac{1+a_\perp^2}{(1+\phi)^2} - 1\right] \\ &\quad + H(\xi-\xi_i)\frac{(1-\alpha)}{2}\left[\frac{1+a_\perp^2}{(1-\phi(\xi_i)+\phi)^2} - 1\right], \end{aligned} \tag{B9}$$

where it is assumed the electrons are born at a phase peak of the laser electric field, i.e., $a_\perp(\xi_i) = 0$. The above wave equation may be used for the investigation of the wakefield modification in a high-Z gas undergoing ionization.

Figure 16 illustrates the ionization effect on the wakefield generation. To avoid the electron beam loading effect on the wakefield, according to Fig. 12(c), we use the laser intensity of $a_0 = 1.6$ here. The red/gray solid line shows the wakefield when pure pre-ionized electrons are used ($\alpha = 1.0$). The green/gray dashed-dot line corresponds to $\alpha = 0.95, \xi_i - \xi_{Lpeak} = 0.0$, where ξ_{Lpeak} represents the position of the laser peak. The black dashed-dot line, which almost overlaps with the red/gray solid line, corresponds to $\alpha = 0.95, \xi_i - \xi_{Lpeak} = 1.0\lambda_p$. The black solid line corresponds to $\alpha = 0.95, \xi_i - \xi_{Lpeak} = -1.0\lambda_p$. The blue/dark gray solid line corresponds to $\alpha = 0.50, \xi_i - \xi_{Lpeak} = 0.0\lambda_p$. From these lines, we see for the current calculation parameters, when the ionization position is before the laser envelope peak, the ionization effect on the wake generation is very weak even when the ionized electron concentration is 5%. However, the ionization effect is obvious once the ionization position is at or behind the laser envelope peak. Note that the ionization for hydrogen (at laser intensity $\sim 10^{14}$ W/cm^2) is

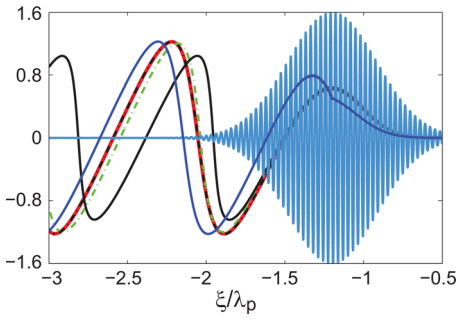

FIG. 16. (Color online) Ionization effect on wakefield generation. The light blue/gray line shows the normalized laser electric field. The other lines show the wakefield intensity ($E_x \times 60$, see text). The normalized laser intensity $a_0 = 1.6$ and length of $L_{FWHM} = 14.89T_0$ are considered. The total electron density is $n_e = 0.001n_c$.

far in front of the laser peak, and the effect on wake generation is negligible. In our previous examples, ionization of nitrogen mainly happens before the laser peak (see Fig. 4) and the later ionized electron concentration is around 5%; hence, the ionization effect on the wakefield generation is also negligible. However, when the concentration increases further, the ionization effect appears as shown by the blue/dark gray solid line in Fig. 16. The second bucket has been moved back compared with the low concentration case. From our calculation results, we see generally the wakefield structure is more sensitive on the ionization position than the concentration of the later ionized electrons once $\alpha > 0.75$.

[1]E. Esarey, C. B. Schroeder, and W. P. Leemans, Rev. Mod. Phys. **81**, 1229 (2009).
[2]F. Gruener, S. Becker, U. Schramm, T. Eichner, M. Fuchs, R. Weingartner, D. Habs, J. Meyer-ter-Vehn, M. Geissler, M. Ferrario L. Serafini, B. van der Geer, H. Backe, W. Lauth, and S. Reiche, Appl. Phys. B **86**, 431 (2007).
[3]C. B. Schroeder, W. M. Fawley, F. Grueuner, M. Bakeman, K. Nakamura, K. E. Robinson, C. Toth, E. Esarey, and W. P. Leemans, *Advanced Accelerator Concepts*, edited by C. B. Schroeder, E. Esarey, and W. Leemans (AIP, New York, 2009), Vol. **1086**, p. 637C642.
[4]C. B. Schroeder, E. Esarey, C. G. R. Geddes, C. Benedetti, and W. P. Leemans, Phys. Rev. ST Accel. Beams **13**, 101301 (2010).
[5]W. P. Leemans, B. Nagler, A. J. Gonsalves, C. Toth, K. Nakamura, C. G. R. Geddes, E. Esarey, C. B. Schroeder, and S. M. Hooker, Nature Phys. **2**, 696 (2006).
[6]K. Nakamura, B. Nagler, C. Toth, C. G. R. Geddes, C. B. Schroeder, E. Esarey, W. P. Leemans, A. J. Gonsalves, and S. M. Hooker, Phys. Plasmas **14**, 056708 (2007).
[7]E. Esarey, R. F. Hubbard, W. P. Leemans, A. Ting, and P. Sprangle, Phys. Rev. Lett. **79**, 2682 (1997).
[8]C. B. Schroeder, P. B. Lee, J. S. Wurtele, E. Esarey, and W. P. Leemans, Phys. Rev. E **59**, 6037 (1999).
[9]G. Fubiani, E. Esarey, C. B. Schroeder, and W. P. Leemans, Phys. Rev. E **70**, 016402 (2004).
[10]H. Kotaki, S. Masuda, M. Kando, J. K. Koga, and K. Nakajima, Phys. Plasmas **11**, 3296 (2004).
[11]S. Bulanov, N. Naumova, F. Pegoraro, and J. Sakai, Phys. Rev. E **58**, R5257 (1998).
[12]P. Tomassini, M. Galimberti, A. Giulietti, D. Giulietti, L. A. Gizzi, L. Labate, and F. Pegoraro, Phys. Rev. ST Accel. Beams **6**, 121301 (2003).
[13]A. V. Brantov, T. Z. Esirkepov, M. Kando, H. Kotaki, V. Y. Bychenkov, and S. V. Bulanov, Phys. Plasmas **15**, 073111 (2008).
[14]J. Faure, C. Rechatin, A. Norlin, A. Lifschitz, Y. Glinec, and V. Malka, Nature **444**, 737 (2006).
[15]H. Kotaki, I. Daito, M. Kando, Y. Hayashi, J. Ma, L.-M. Chen, T. Z. Esirkepov, Y. Fukuda, T. Homma, A. Pirozhkov, J. K. Koga, K. Nakajima, H. Daido, and S. V. Bulanov, IEEE Trans. Plasma Sci. **36**, 1760 (2008).
[16]C. Rechatin, J. Faure, A. Ben-Ismail, J. Lim, R. Fitour, A. Specka, H. Videau, A. Tafzi, F. Burgy, and V. Malka, Phys. Rev. Lett. **102**, 164801 (2009).
[17]T.-Y. Chien, C.-L. Chang, C.-H. Lee, J.-Y. Lin, J. Wang, and S.-Y. Chen, Phys. Rev. Lett. **94**, 115003 (2005).
[18]C. G. R. Geddes, K. Nakamura, G. R. Plateau, Cs. Toth, E. Cormier-Michel, E. Esarey, C. B. Schroeder, J. R. Cary, and W. P. Leemans, Phys. Rev. Lett. **100**, 215004 (2008).
[19]K. Schmid, A. Buck, C. M. S. Sears, J. M. Mikhailova, R. Tautz, D. Herrmann, M. Geissler, F. Krausz, and L. Veisz, Phys. Rev. ST Accel. Beams **13**, 091301 (2010).
[20]J. Faure, C. Rechatin, O. Lundh, L. Ammoura, and V. Malka, Phys. Plasmas **17**, 083107 (2010).
[21]A. J. Gonsalves, K. Nakamura, C. Lin, D. Panasenko, S. Shiraishi, T. Sokollik, C. Benedetti, C. B. Schroeder, C. G. R. Geddes, J. van Tilborg, J. Osterhoff, E. Esarey, C. Toth, and W. P. Leemans, Nature Phys. **7**, 862 (2011).
[22]D. Umstadter, J. K. Kim, and E. Dodd, Phys. Rev. Lett. **76**, 2073 (1996).
[23]M. Chen, Z.-M. Sheng, Y.-Y. Ma, and J. Zhang, J. Appl. Phys. **99**, 056109 (2006).
[24]C. McGuffey, A. G. R. Thomas, W. Schumaker, T. Matsuoka, V. Chvykov, F. J. Dollar, G. Kalintchenko, V. Yanovsky, A. Maksimchuk, K. Krushelnick, V. Y. Bychenkov, I. V. Glazyrin, and A. V. Karpeev, Phys. Rev. Lett. **104**, 025004 (2010).
[25]A. Pak, K. A. Marsh, S. F. Martins, W. Lu, W. B. Mori, and C. Joshi, Phys. Rev. Lett. **104**, 025003 (2010).
[26]C. E. Clayton, J. E. Ralph, F. Albert, R. A. Fonseca, S. H. Glenzer, C. Joshi, W. Lu, K. A. Marsh, S. F. Martins, W. B. Mori, A. Pak, F. S. Tsung, B. B. Pollock, J. S. Ross, L. O. Silva, and D. H. Froula, Phys. Rev. Lett. **105**, 105003 (2010).
[27]E. Esarey and M. Pilloff, Phys. Plasmas **2**, 1432 (1995).
[28]C. B. Schroeder, E. Esarey, B. A. Shadwick, and W. P. Leemans, Phys. Plasmas **13**, 033103 (2006).
[29]K. A. Marsh, C. E. Clayton, C. Joshi, W. Lu, W. B. Mori, A. Pak, L. O. Silva, N. Lemos, R. A. Fonseca, S. de Freitas Martins, F. Albert, T. Doeppner, C. Filip, D. Froula, S. H. Glenzer, D. Price, J. Ralph, and B. B. Pollock, in Proceedings of 2011 Particle Accelerator Conference, New York, NY, USA, TUOBN1; J. E. Ralph, C. E. Clayton, F. Albert, B. B. Pollock, S. F. Martins, A. E. Pak, K. A. Marsh, J. L. Shaw, A. Till, J. P. Palastro, W. Lu, S. H. Glenzer, L. O. Silva, W. B. Mori, C. Joshi, and D. H. Froula, Phys. Plasmas **17**, 056709 (2010).
[30]W. P. Leemans, C. E. Clayton, W. B. Mori, K. A. Marsh, A. Dyson, and C. Joshi, Phys. Rev. Lett. **68**, 321 (1992).
[31]A. Pukhov, J. Plasma Phys. **61**, 425 (1999).
[32]M. V. Ammosov, N. B. Delone, and V. P. Krainov, Sov. Phys. JETP **64**, 1191 (1986).
[33]N. B. Delone and V. P. Krainov, J. Opt. Soc. Am. B **8**, 1207 (1991).
[34]W. P. Leemans, P. Catravas, E. Esarey, C. G. R. Geddes, C. Toth, R. Trines, C. B. Schroeder, B. A. Shadwick, J. van Tilborg, and J. Faure, Phys. Rev. Lett. **89**, 174802 (2002).
[35]C. B. Schroeder, E. Esarey, C. G. R. Geddes, C. Toth, B. A. Shadwick, J. van Tilborg, J. Faure, and W. P. Leemans, Phys. Plasmas **10**, 2039 (2003).
[36]A. Pukhov and J. Meyer-ter-Vehn, Appl. Phys. B **74**, 355 (2002).
[37]I. Kostyukov, A. Pukhov, and S. Kiselev, Phys. Plasmas **11**, 5256 (2004).
[38]E. Esarey, B. A. Shadwick, P. Catravas, and W. P. Leemans, Phys. Rev. E **65**, 056505 (2002).
[39]B. B. Pollock, C. E. Clayton, J. E. Ralph, F. Albert, A. Davidson, L. Divol, C. Filip, S. H. Glenzer, K. Herpoldt, W. Lu, K. A. Marsh, J. Meinecke, W. B. Mori, A. Pak, T. C. Rensink, J. S. Ross, J. Shaw, G. R. Tynan, C. Joshi, and D. H. Froula, Phys. Rev. Lett. **107**, 045001 (2011); J. S. Liu, C. Q. Xia, W. T. Wang, H. Y. Lu, C. Wang, A. H. Deng, W. T. Li, H. Zhang, X. Y. Liang, Y. X. Leng, X. M. Lu, C. Wang, J. Z. Wang, K. Nakajimia, R. X. Li, Z. Z. Xu, Phys. Rev. Lett. **107**, 035001 (2011).
[40]C. B. Schroeder, E. Esarey, E. Cormier-Michel, and W. P. Leemans, Phys. Plasmas **15**, 056704 (2008).
[41]A. J. Kemp, R. E. W. Pfund, and J. Meyer-ter-Vehn, Phys. Plasmas **11**, 5648 (2004).